D137
9/13/83

(NASA-CR-173172) X-RAY SENSOR DEVELOPMENT FOR MAGNETOSPHERIC RESEARCH Final Report (Lockheed Missiles and Space Co.) 38 p HC A03/MF A01 CSCL 14B

N84-16525

Unclas
G3/35 15139

X-RAY SENSOR DEVELOPMENT FOR MAGNETOSPHERIC RESEARCH

Final Report Submitted to: NASA
Office of Space Sciences
Solar Terrestrial Division
Space Plasma Physics Program Office
Code ST-5
Washington, D.C. 20546

Submitted by:

Dr. William L. Imhof, Principal Investigator
Org. 52-12, Bldg. 255
Lockheed Palo Alto Research Laboratory
3251 Hanover Street
Palo Alto, California 94304
(415) 858-4052

Sept. 1983

OUTLINE OF REPORT

1. ACKNOWLEDGEMENTS

The following members of the Space Sciences Laboratory at Lockheed Palo Alto Research Laboratory made significant contributions to the effort reported here: Drs. J. R. Kilner, J. B. Reagan, D. W. Datlowe and G. H. Nakano.

I. SUMMARY

The effort performed here has been directed toward the long-range goal of improving the state of the art for future geophysical bremsstrahlung x-ray imagers. The ARPA-301 data on the P78-1 satellite were processed to obtain detailed information on the long-term x-ray environment; specifically, the distributions in total x-ray intensities and energy spectral parameters and the spatial extents of the x-ray sources. The spacecraft was in a noon-midnight orbit at ~ 600 km so the local time coverage of the bremsstrahlung x-ray measurements spanned an interval of about $\pm$ 2 hours around noon and midnight. The average x-ray intensity near noontime is found to decrease with increasing local time whereas the opposite trend occurs around midnight. At both of these local times the average flux increases with increasing level of geomagnetic activity. The distributions in flux are also considered for given local time intervals and these span a large dynamic range. The temporal correlation between the x-ray flux in different local time sectors is found to decrease with increasing difference in local time. The average spectral shapes do not depend significantly upon local time or geomagnetic activity.

The analyses have shown the need in future x-ray instrumentation to be able to accept a wide variability in x-ray fluxes and spectral shapes and the analyses have demonstrated the complexity of the x-ray environment and hence the parent electron precipitation environment. From this investigation it is clear that in the future experimenters must continually stay abreast of the latest measurements. The distribution in x-ray fluxes and spectral shapes presented here are of particular importance for evaluating conceptual instrument designs. Even for consideration of fine-angular-resolution imaging these fluxes and spectral parameters averaged over relatively wide solid angles provide important

check-points for evaluating frequencies of occurrence of various hypothesized x-ray images. For example, in the future it is proposed to apply such considerations to the PIXIE x-ray imager on the OPEN program.

II. INTRODUCTION

Bremsstrahlung x-ray measurements make possible the remote sensing of energetic electron deposition from the magnetosphere into the upper atmosphere. An x-ray detector on a satellite in the proper orbit can, by remote sensing, give global information about spatial an temporal variations in this electron deposition. To date studies of the magnetospheric electron population have been carried out by intercepting the electrons at single points in space. Worldwide imaging capability is essential for the next generation of understanding of the coupling between the magnetosphere and the upper atmosphere.

The performance of x-ray imaging is now proven but the technology is young: long sensor lifetimes require conservative approaches, and considerable potential for optimization remains in the quality of data to be obtained. By detailed analysis of several key factors, the instrument cost, weight, range, sensitivity, and reliability can be improved. The present effort has been directed toward ways to improve the technology even further. With the availability of several years of flight data with a variety of bremsstrahlung x-ray detectors the Space Sciences Laboratory at LPARL has had the unique opportunity to obtain detailed mappings of the flux and spectral distributions in the near earth space which can form the basis for future detailed instrument designs.

The first satellite measurements of bremsstrahlung x-rays, which were performed by the Lockheed Group (Imhof et al., 1974), demonstrated the feasibility of the technique and emphasized the advantages. Mappings of the spatial distributions of x-rays were obtained. However, these first observations were performed with a single wide angle germanium detector on a spinning satellite so the spatial resolution was quite limited and the x-ray threshold energy was rather high, ~ 50 keV. In a subsequent flight (Mizera et al., 1978) the threshold energy was lowered to ~1.4 keV, thus providing better coverage of auroral precipitation processes, but again the spatial resolution was rather coarse.

Beginning in 1979 the Lockheed group (Imhof et al., 1980) has been obtaining x-ray mappings from the P78-1 satellite at an altitude of 600 km with an array of cadmium telluride spectrometers. The latter instrumentation represents a major improvement in spatial mapping capability. However, the angular resolution is less than that required for magnetospheric studies at higher altitudes and only coarse (6 channel) energy spectrum measurements are performed.

A proportional counter x-ray imaging spectrometer was flown in 1982 by the Lockheed group on the USAF S81-1 polar orbiting spacecraft under the U.S. Navy-sponsored SEEP program. The X-ray imaging spectrometer (XRIS) measured x-rays from the atmosphere with a large area imaging proportional counter sensitive over the energy range 4 to 40 keV. The XRIS field of view is divided into 16 pixels in the direction perpendicular to the satellite trajectory. This enables the remote sensing of electron precipitation over a large area with fine spatial (30 km) and temporal (0.13 sec) resolution.

In December 1982 an x-ray proportional counter with 24 differential energy channels between 2 and 100 keV was flown on a DMSP polar orbiting satellite by the Aerospace Group. Auroral x-ray images are obtained by scanning mechanically.

Techniques for measuring x-rays from a satellite with very fine angular resolution have been developed extensively for x-ray astronomy purposes and for solar studies. However, in these applications ultra-fine angular resolution is usually sought over an extremely limited field of view for a given energy. When measuring bremsstrahlung x-rays from the precipitation of electrons of magnetospheric origin a much wider field of view is needed with less severe angular resolution requirements and with far greater energy range and resolution. The direct applicability of x-ray astronomy instrumentation to magnetospheric studies is thus quite limited. Also, for many magnetospheric applications a higher sensitivity is needed to cover weak events. The energy deposited into the atmosphere by energetic electrons is an important magnetospheric parameter which can be sensed remotely by x-ray imaging spectrometers. Because of this capability x-ray detectors have become mandatory instrumentation on future (polar-orbiting) space plasma physics missions.

The effort performed here has been directed toward the long-range goal of improving the state of the art for future geophysical x-ray detectors. Specifically, we have processed ARPA-301 data on the P78-1 satellite to obtain detailed information on the long-term x-ray environment. Here we present results from the data analyses on the following quantities: 1) long-term distributions in total x-ray intensities, 2) long-term distributions in x-ray energy spectral parameters and 3) the local time extents of the x-ray sources. Comparisons were made with other satellite data to obtain more information on the selective sensitivities and backgrounds with different instrument designs.

III. BREMSSTRAHLUNG X-RAY DATA FROM THE P78-1 SATELLITE

1. Description of Experiment

The Lockheed Palo Alto Research Laboratory has a satellite bremsstrahlung x-ray data base spanning a period of several years. Approximately 6 months of data were acquired in 1972-73 from the first satellite-borne bremsstrahlung x-ray experiment flown on the P72-1 vehicle. The P78-1 satellite was launched into polar orbit at ~ 600 km altitude on 24 February 1979 and as of August 1983 x-ray mappings are still being acquired with an array of cadmium telluride spectrometers on board. These instruments are known by the acronym GEMS (Gamma-ray Environment Mapping Spectrometer). The satellite spins with a period of 5.5 seconds about an axis perpendicular to the orbit plane and pointed eastward at the ascending node so that the array of eight x-ray detectors oriented at selected view angles with respect to the spacecraft spin axis provides fine-scale mappings of the sources of x-rays > 21 keV. To economize on weight and volume, two cadmium telluride sensors are placed in each of four cesium iodide anticoincidence shields. Each of the CdTe sensors has a viewing aperture of $\pm 40^{\circ}$ along the spin direction. Four of the sensors, which are oriented at central view angles of 10° and 30° to the right and left of the plane have a collimation of $\pm 10^{\circ}$ perpendicular to the spin direction. The other four sensors, which are oriented at 44° and 50° to the right and left, have a collimation of $\pm 6^{\circ}$. Thus, the complete set provides nearly horizon-to-horizon coverage. The rectangular CdTe sensors are 2 mm thick and 7 x 22 mm in area. From laboratory measurements with radioactive sources we found that the active areas of those selected for flight varies from 0.98 to 1.22 cm^2. The geometric factors are ~ 0.40 cm^2 sr for the detectors at 10° and 30° and are ~ 0.24 cm^2 sr for those at 44° and 56°. A few days after launch one of the double

CdTe units experienced a failure. However, an extensive set of data has been acquired with six CdTe mapping sensors. At any given instant a spectrometer can view at most only a portion of its full zone, and it requires ~ 3 seconds for the field of view to sweep completely across the path.

Frequently when the satellite is poleward of the radiation belts, the counting rates in the cadmium telluride detectors are close to the normal background level, which includes contributions from the diffuse cosmic x-ray spectrum when the spectrometer is pointed upward and from atmospheric gamma rays when viewing downward. Sometimes, however, significant fluxes of bremsstrahlung x-rays are observed when the CdTe spectrometers are pointed toward a region of the upper atmosphere.

The existing bremsstrahlung x-ray data acquired from satellites clearly demonstrate the wide variety of intensities, spectral shapes, spatial distributions and temporal variations encountered. Clearly a large body of data is required for any environmental studies. Under the program performed here, the P78-1 satellite bremsstrahlung x-ray data have been processed to obtain x-ray intensities, angular distributions and energy spectra for x-rays of $\geq$ 21 keV energy.

For the data considered here, the threshold levels for signal analysis were set by command at 21 keV and the channels covered the following x-ray energy ranges: 21-30 keV, 30-46, 46-68 keV, 68-98 keV, 98-139 keV, and > 139 keV. The total counts in each of the energy intervals from each of the CdTe sensors were recorded once every 0.032 s, during which period the satellite rotated just over 2^{o} about the spin axis. In the events presented here, most of the bremsstrahlung x-ray counts were recorded in the lowest three channel intervals, covering the range 21-68 keV. For these channels, in order of increasing energy, the average photon detection efficiencies, including transmission through the

1 g/cm^2 CH_2 absorber for stopping electrons in the collimator, have been calculated by a Monte Carlo technique to be 0.67, 0.66, and 0.77 respectively.

The relative gains of the different spectrometers were monitored on orbit through various intercomparisons, including observations of the diffuse cosmic x-ray spectrum. In the latter comparisons the diffuse cosmic ray counting rates in the second, third, and fourth channels in each unit all agree with each other and with published values [Kinzer et al., 1978] within about 10%; this observation combined with the spectrum shape leads to the conclusion that all of the gains are within about 5% of each other and of the prelaunch calibrations.

2. Processing of the Data

Flight data from the ARPA-301 payload on the P78-1 spacecraft were digitized under the sponsorship of the Air Force and merged with ephemeris information. Since hundreds of tapes are involved and a large fraction of the data stream involves sensors that are not of great importance for magnetospheric physics studies the x-ray and particle data were written in compressed form at the Lockheed Palo Alto Research Laboratory on separate tapes. Under this program, in order to make use of the large body of bremsstrahlung x-ray data these tapes were then further combined and compressed into two magnetic tapes. These compressed data were used for the present investigation.

For statistical studies of the bremsstrahlung x-ray production certain assumptions were made in the interests of simplicity. All x-ray data were taken from measurements performed when the satellite was at a position just poleward of the radiation belts.

IV. LONG-TERM DISTRIBUTIONS IN THE X-RAY ENVIRONMENT

Bremsstrahlung x-ray data from the GEMS spectrometers were processed in longitude intervals selected to provide an optimum and reasonably consistent geometry for observing bremsstrahlung x-rays produced near the trapping boundary from satellite positions just poleward of that boundary where the local fluxes of particles are quite low. The longitude intervals at an L shell of 5 were as follows: 175°E to 265°E on the nightside in the northern hemisphere, 290°E to 30°E on the dayside in that hemisphere; 120°E to 170°E on the nightside in the southern hemisphere and 30°E to 120°E on the southern dayside. Over these longitude intervals the satellite path is approximately perpendicular to the various high latitude L shell contours. With these criteria data were available for analysis from 492 passes of the P78-1 satellite. To insure adequate coverage of any precipitation regions spin averaged counting rates were used. Backgrounds were subtracted based on measurements performed during quiet passes.

In Figure 1 the observed x-ray fluxes are plotted as a function of local time, separately for geomagnetically disturbed conditions when Dst was below -32 and for relatively quiet conditions when Dst was above -33. These fluxes were obtained by dividing the spin-averaged efficiency-corrected counting rates measured in each instrument by its geometric factor and the resulting quantities therefore represent the fluxes averaged over a wide solid angle. The geometries for each of the two sets of detectors Da and Db viewing to the far left are nearly identical to those for Ca and Cb viewing to the far right, and should therefore not affect significantly the relative intensities of x-rays emitted from the earliest and latest local times. Also the electronic gains of the two systems do not differ significantly since the background spectra and counting rates in the second, third and fourth channels in the C and D detectors agree with each other and are within about 10% of the published cosmic ray intensities as discussed elsewhere in this report. In the first channel the scatter in background counting rate among the 6 detectors is greater, but they still span a total dynamic range of less than a factor of two and there appears to be no systematic difference between the C detectors and the D detectors, for example. For a more quantitative appraisal of the emitted x-ray intensities versus local time the counting rates should be normalized to a standard source to detector distance, assuming an R^{-2} variation (e.g. Imhof et. al., 1982). The extreme limits of such a normalization factor are generally within a factor of 2. It is clear that for times near noon the x-ray intensities decrease with increasing local time whereas the opposite is true near midnight. These local time trends appear to be consistent with the average absorption distributions presented by Berkey et. al. (1974) based on 60 auroral absorption substorms.

In the left section of Figure 2A the x-ray counting rates are plotted as a function of the Dst index for the pair of detectors Da + Db, separately for noon and midnight passes. The x-ray flux and hence the intensity of precipitating electrons tends to increase with increasing negative value of the Dst index, although the data show considerable scatter. This trend may be somewhat stronger and more clear cut on the nightside than on the dayside. The same data are plotted as a function of AE and of K_p in the middle and right hand sections, respectively. As with the Dst index the trends are perhaps more clearcut on the nightside and the x-ray fluxes are greater at times of increased geomagnetic activity. Similar trends appear in the measurements performed with each of the detectors, but for simplicity of presentation only the data for detectors Da + Db are shown. It is not clear that any one of the indices (Dst, AE or K_p) organizes the x-ray intensities better than the others.

So far we have considered the average x-ray fluxes observed under various local time and geomagnetic activity conditions. For many purposes, including evaluations of possible instrument designs for future satellite bremsstrahlung x-ray measurements, it is worthwhile to have available the distributions in x-ray fluxes observed under various conditions. For example, one may need to know what percentage of the time the flux is above a given value. With that consideration in mind the distributions in counting rate are plotted in Figure 2B for the pair of detectors Da + Db, separately for noon and midnight passes. Clearly, the counting rates span a wide interval about the average or median values.

One important feature of an x-ray event is the spatial or local time extent of the bremsstrahlung x-ray sources. Equivalently, one can ask how far apart the x-ray sources can be located and still be correlated with each other in intensity. This subject might best be addressed by considering the degree of correlation in counting rate between the different x-ray detectors in the GEMS array. Correlation coefficients have been calculated between the counting rates observed in the various detectors. Two representative examples of plots of the counting rate in one detector versus that in another are shown in Figures 3A and 3B. For comparison straight lines indicating a one to one correspondence between the two detectors are shown. These plots strongly indicate that the counting rates in two adjacent detectors (Ca and Cb) are better correlated with each other than for detectors at opposite ends of the array (Cb and Db).

The variation with difference in local time in the degree of correlation between various sensors is best considered by calculating correlation coefficients between the counting rates measured in the sensors. The correlation coefficients are plotted in Figure 4 as a function of the number of units separating the pairs of sensors, separately for the day and night passes, and for both combined. Median values of the correlation coefficient at each separation distance are connected by straight lines. Clearly, the correlation decreases with increasing separation distance at a similar rate for both noontime and midnight observations.

Next let us consider the variations with geomagnetic activity in the shapes of the energy spectra. X-ray energy spectra were derived from the measured energy loss spectra by using the detection efficiencies quoted earlier in the paper. For all cases meeting a minimum statistical criterion, least-squares fits were made to the observed x-ray energy spectra, assuming exponential spectrum shapes. The minimum criterion required that there be at least 10 counts in the first channel after background subtraction. The known relationship between the energy spectra of the precipitating electrons and the measured x-ray spectra (e.g Walt et al., 1979) is such that harder x-ray spectra correspond to harder electron spectra. From the measured x-ray spectra exponential e-fold energies, E_o, were derived based on the counts recorded in the three lowest energy channels; 21-30 keV, 30-46 keV and 46-68 keV. In Figure 5 these e-fold energies are plotted as a function of the Dst index. Overall, the spectra show no clear trends with level of geomagnetic activity at either nighttime or daytime and the data display considerable scatter.

The x-ray spectral trends with local time are illustrated in Figure 6 where values of E_o are plotted as a function of local time, separately for relatively normal periods (taken to be at values of Dst above -30) and disturbed intervals (when Dst is less than -30). Significant trends are not found under either normal or disturbed conditions and for times near either noon or midnight. This finding, however, does not preclude a dependence upon Dst of the occurrence of hard events. In order to consider that possibility we have plotted in Figure 7 the distributions in E_o at E_o > 20 keV for three selected ranges in Dst.

Let us next consider the observed variations of spectral shape with intensity. In Figure 8 the x-ray intensity (counts/sec-cm^2-sr-keV) in channel 1, which has a central energy of ~ 25.5 keV, is plotted as a function of the least-squares fit e-fold energy E_o. The values of E_o obtained on each pass of the satellite are plotted individually, separately for each of four time intervals: before noon, after noon, before midnight and after midnight. The large scatter in the individual points makes it difficult to identify trends. Therefore, in order to consider any trends more quantitatively the distributions in E_o value for each of several flux levels are provided in Figure 9. It appears that at times of higher intensity of x-rays in the first channel the energy spectrum tends to be softer. This result is consistent with the findings of Barcus and Rosenberg (1966) that the spectrum of x-rays, on the average, steepens with increasing differential x-ray intensity around 70 keV.

From the data just presented certain conclusions can be drawn. These may be classified into the observed variations with local time and geomagnetic activity in both the x-ray intensities and the x-ray spectral shapes.

The findings are summarized as follows:

1) X-Ray Intensities

* On the average the x-ray intensity decreases with increasing local time near noon and increases with increasing local time near midnight for both disturbed and quiet times.
* On the average the x-ray fluxes near both noon and midnight increase with increasing level of geomagnetic activity.
* The correlation of intensities in different local time sectors decreases with increasing difference in local time.

2) X-Ray Energy Spectra

* The average spectral shapes do not change significantly with local time.
* At times of higher intensity of x-rays at ~ 25 keV the energy spectrum tends to be softer.
* No clear trends are present for variation of the average spectral shape with geomagnetic activity level, at times near either noon or midnight.

V. FUTURE INSTRUMENT DESIGN CONSIDERATIONS

In the future evolution of bremsstrahlung x-ray imagers for magnetospheric investigations, one of the most critically needed improvements is in the area of background suppression. The background counting rates frequently determine the sensitivity of a spectrometer for measuring bremsstrahlung x-rays. Significant backgrounds associated with cosmic ray particle interactions in the instrument may be present even when the satellite is not in the radiation belts. Also, depending on the viewing geometry the gamma rays produced in the atmosphere by cosmic ray interactions and the fluxes of diffuse x-rays from outer space may add significantly to the backgrounds. These points can be illustrated with some data acquired with the GEMS spectrometers on the low altitude polar orbiting satellite P78-1. Fortunately for this purpose the satellite is spinning so that at any given location measurements are obtained of the backgrounds from outer space as well as those emitted from the atmosphere.

In Figure 10 the counting rates above 21 keV are plotted as a function of the orientation angle of the spectrometers at selected L shells, all at relatively quiet times when electron precipitation rates were a minimum and the fluxes of bremsstrahlung x-rays were therefore very low. The counting rates shown represent minimum values recorded in each L shell region. The minimum counting rates when the spectrometer was viewing in the downward direction are plotted as a function of L value in Figure 11. One can see that the minimum or background counting rates are higher by about a factor of 2 over the polar cap than at low latitudes, consistent with their being associated with cosmic rays. At intermediate L values the counting rates are higher, indicating a possible association with the radiation belts.

The background energy spectra measured with the GEMS spectrometers when pointed to outer space are shown in Figure 12. These spectra are presented as absolute fluxes with proper account taken of the geometric factors and efficiencies. For comparison, the known diffuse cosmic ray spectrum as published by Kinzer et al. (1978) is also shown. The spectra in each of the detectors are comparable to the diffuse cosmic ray spectrum and it can therefore be assumed that the local backgrounds were well suppressed. Apparently the design of the GEMS instruments was adequate in regard to background suppression. However, the subject of background rejection is by no means a closed issue, since the anti coincidence shield in the GEMS instrument was relatively large and heavy in comparison to the cadmium telluride sensor and in many future flight opportunities weight and volume are serious limitations. It is therefore very important to achieve a good background rejection at a minimum weight penalty.

Also shown in Figure 12 is the background spectrum measured with one of the germanium spectrometers on the P78-1 satellite. This gamma-ray spectrometer, operating in the range 0.05 to 2.5 MeV, consisted of a single large (85 cm^3) IGe detector shielded by a NaI anticoincidence shield. The germanium detector was approximately 5 cm in diameter by 4.5 cm in length and surrounded by a 5 cm thick NaI scintillator. The instrument aperture was a cone with a 45^o half angle and was also shielded against charged particles with a 1.27 cm thick plastic scintillator. As with the GEMS spectrometers the relatively thick anti-coincidence shield and wide angle aperture both help in providing a very favorable diffuse cosmic ray to background response ratio at the lower energies. Either of these detectors is clearly very favorable for measuring bremsstrahlung x-rays of magnetospheric origin as indicated by the low background response. However, the detectors typically span a region wider than the source of bremsstrahlung x-rays and so some additional background arises from the atmospheric gamma ray sources. With a somewhat narrower field of view the response to bremsstrahlung x-rays would be optimized. With the even finer angular opening needed for bremmstrahlung x-ray mappings the backgrounds become relatively more important and their further suppression may be necessary.

It is becoming increasingly important to minimize the total weight and volume occupied by bremsstrahlung x-ray spectrometers to be flown on future missions such as OPEN. One, therefore, may not be able to afford the luxury of using a heavy cesium iodide anti-coincidence shield as with the GEMS instrument on the P78-1 satellite. Lighter weight anti-coincidence shields must be considered and their geometric designs carefully evaluated.

VI. CONCLUSIONS AND RECOMMENDATIONS

The findings of the data analysis effort can be summarized as follows:

1) Long-term distributions in x-ray intensities

- On the average the x-ray fluxes (21 - 68 keV) near both noon and midnight increase with increasing level of geomagnetic activity, although major deviations from this pattern occur.
- On the average the x-ray fluxes (21 - 68 keV) decrease with increasing local time near noon and increase with increasing local time near midnight for both geomagnetically disturbed and quiet times.

2) Long-term distributions in x-ray energy spectral parameters

- The average spectral shapes do not depend significantly upon local time.
- The level of geomagnetic activity has little effect on the average spectral shape, at times near either noon or midnight.
- The x-ray energy spectrum tends to be softer at times of higher fluxes of x-rays near 25 keV.

3) Local time extents of the x-ray sources

- The correlation of x-ray intensities at different local times decreases with increasing difference in local time.

Existing satellite data have indicated that the reduction of backgrounds is one of the most critically needed improvements in the design of bremsstrahlung x-ray imagers for magnetospheric investigations. The sensitivity of an instrument is often strongly dependent upon the background levels. For these considerations data have been used from past satellite programs in which spectrometers were flown with a variety of sensing elements, including cadmium telluride and germanium. These previously flown instruments have clearly demonstrated that if an adequate weight penalty can be paid then locally produced backgrounds can generally be reduced to a level where the atmospheric gamma ray or diffuse cosmic x-ray intensities are the dominant source of background provided the instrument is not in the radiation belts and that extremely narrow x-ray collimation is not desired.

The x-ray environment data presented here should be very helpful in planning future bremsstrahlung x-ray measurements and in designing the instrumentation. The data analyses have shown that future x-ray instrumentation must be able to:

- Accept a wide variability in x-ray fluxes.
- Map x-ray sources that are often localized to local time differences of only a few tenths of an hour.

Of particular importance in the results of the data analyzed here are the average x-ray fluxes and their distributions observed at various local times and the distributions in best-fit E_o spectral values. Even for consideration of fine-angular resolution imaging these fluxes and spectral parameters averaged over relatively wide solid angles provide important check-points for evaluating frequencies of occurrence of various hypothesized x-ray images. For example, it is planned to make this type of comparison with the x-ray model presently being used for design and evaluation of the PIXIE x-ray imager on the OPEN program.

Perhaps most important, the data considered here have demonstrated the complexity of the x-ray environment and the important need in this rapidly evolving field of bremsstrahlung x-ray imagery for experimenters to stay abreast of the latest measurements.

FIGURE CAPTIONS

Figure 1 Observed x-ray fluxes versus local time, shown separately for Dst < -32 and for Dst > -33.

Figure 2A X-ray counting rates near noon and midnight for each of three different geomagnetic indices. These plots are all for one pair of detectors, Da + Db.

Figure 2B Cumulative distributions in counting rate in the first 3 channels of detectors DA and DB for each of two local time intervals.

Figure 3(A) The x-ray counting rate in the Cb detector plotted as a function of the simultaneous counting rate in the Db detector.

Figure 3(B) The x-ray counting rate in the Cb detector plotted as a function of the simultaneous counting rate in the Ca detector.

Figure 4 The correlation coefficients plotted as a function of the number of units separating the pairs of sensors.

Figure 5 Exponential e-fold energies, E_o, for the measured x-ray spectra plotted as a function of the Dst index, separately for noon and midnight passes. The E_o values are averages of least-squares fits to the spectra measured in all of the detectors.

Figure 6 Exponential e-fold energies, E_o, for the measured x-ray spectra plotted as a function of local time, separately for Dst > -30 and Dst < 30. Average least-squares fit E_o values are shown separately for each of the detectors.

Figure 7 Cumulative distributions in E_o value for each of three Dst intervals. In each case the number of observations where $E_o \geq 4.5$ keV has been normalized to 1000.

Figure 8 The x-ray flux in channel 1 plotted as a function of the least-squares fit e-fold energy E_o. Values of E_o obtained on each pass of the satellite are plotted individually, separately for each of four time intervals; before noon, after noon, before midnight and after midnight.

Figure 9 Cumulative distributions in E_o value for each of 6 x-ray flux intervals in channel 1 at 21 - 30 keV. In each case the number of observations where $E_o \geq 4.5$ keV has been normalized to 1000.

Figure 10 Counting rates above 21 keV in the GEMS detector AA plotted as a function of orientation angle at selected L shells.

Figure 11 Minimum counting rates corrected for efficiency when the GEMS spectrometer was viewing in the downward direction.

Figure 12 Background spectra measured with GEMS spectrometers when pointed to outer space.

REFERENCES

Bailey, D. K., Some quantitative aspects of electron precipitation in and near the auroral zone, Reviews of Geophysics, 6, 289, 1968.

Barcus, J. R., and T. J. Rosenberg, Energy spectrum for auroral-zone x-rays 1. Diurnal and type effects. J. Geophys, Res., 71, 803, 1966.

Berkey, F. T., V. M. Driatskiy, K. Henriksen, B. Hultqvist, D. H. Jelly, T. I. Shchuka, A. Theander, and J. Yliniemi, A synoptic investigation of particle precipitation dynamics for 60 substorms in IQSY (1964-1965) and IASY (1969), Planet. Space Sci., 22, 255, 1974.

Bossen, M., R. L. McPherron, and C. T. Russell, A statistical study of Pc 1 magnetic pulsations at synchronous orbit, J. Geophys. Res., 81, 6083, 1976.

Imhof, W. L., J. R. Kilner, G. H. Nakano, and J. B. Reagan, Satellite x-ray mappings of sporadic auroral zone electron precipitation events in the local dusk sector, J. Geophys. Res., 85, 3347, 1980A.

Imhof, W. L. R. W. Nightingale, J. B. Reagan and G. H. Nakano, The morphology of widespread electron precipitation at high latitudes, J. Atm. Terr. Phys. 42, 443, 1980B.

Imhof, W. L., J. Stadsnes, J. R. Kilner, D. W. Datlowe, G. H. Nakano, J. B. Reagan, and P. Stauning, Mappings of energetic electron precipitation following substorm using the satellite bremsstrahlung technique, J. Geophys. Res., 87, 671, 1982.

Kinzer, R. L., W. N. Johnson, and J. D. Kurfess, A balloon observation of the diffuse cosmic x radiation above 20 keV, Astrophys. J., 222, 370, 1978.

Meng, C. I., A. L. Snyder and H. W. Kroehl, Observations of auroral westward traveling surges and electron precipitation, J. Geophys. Res. 83, 575, 1978.

Rosenberg, T. J., L. J. Lanzerotti, D. K. Bailey and J. B. Pierson, Energy spectra in relativistic electron precipitation events, J. Atmos. Terr. Phys., 34, 1977, 1972.

Rosenberg, T. J. and L. J. Lanzerotti, Direct energy inputs to the middle atmosphere, middle atmosphere electro dynamics, report of the workshop on the role of the electrodynamics of the middle atmosphere on solar-terrestrial coupling, NASA CR-2090, page 43, 1979.

Thorne, R. M. and T. R. Larsen, An investigation of relativistic electron precipitation events and their association with magnetopsheric substorm activity, J. Geophys. Res., 81, 5501, 1976.

Walt, M., L. L. Newkirk, and W. E. Francis, Bremsstrahlung produced by precipitating electrons, J. Geophys. Res., 84, 967, 1979.

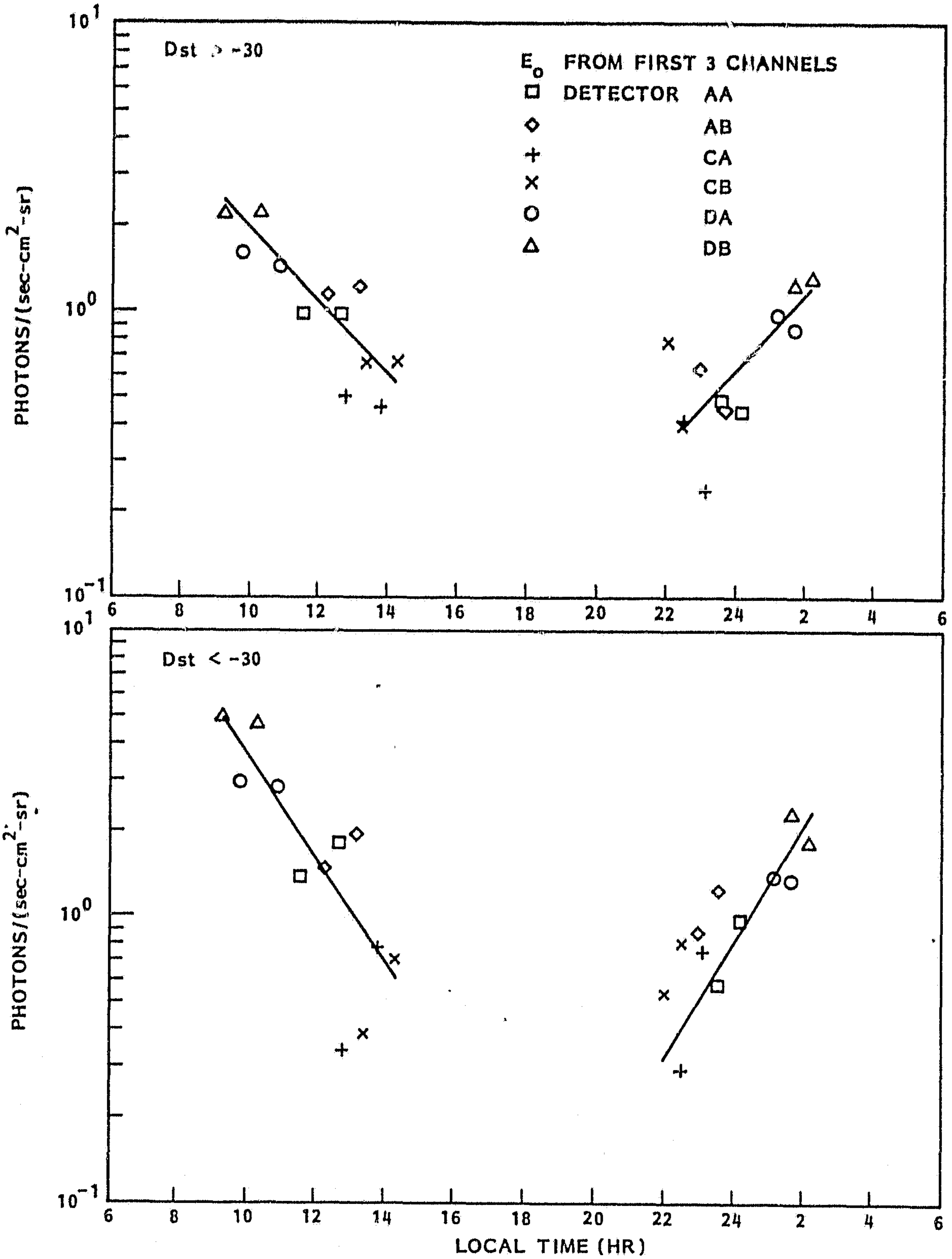
Dst > -30
E_o FROM FIRST 3 CHANNELS
DETECTOR AA
AB
CA
CB
DA
DB
PHOTONS/(sec-cm^2-sr)
10^1
10^0
10^{-1}
Dst < -30
LOCAL TIME (HR)
6 8 10 12 14 16 18 20 22 24 2 4 6

Figure 1

ORIGINAL PAGE IS
OF POOR QUALITY

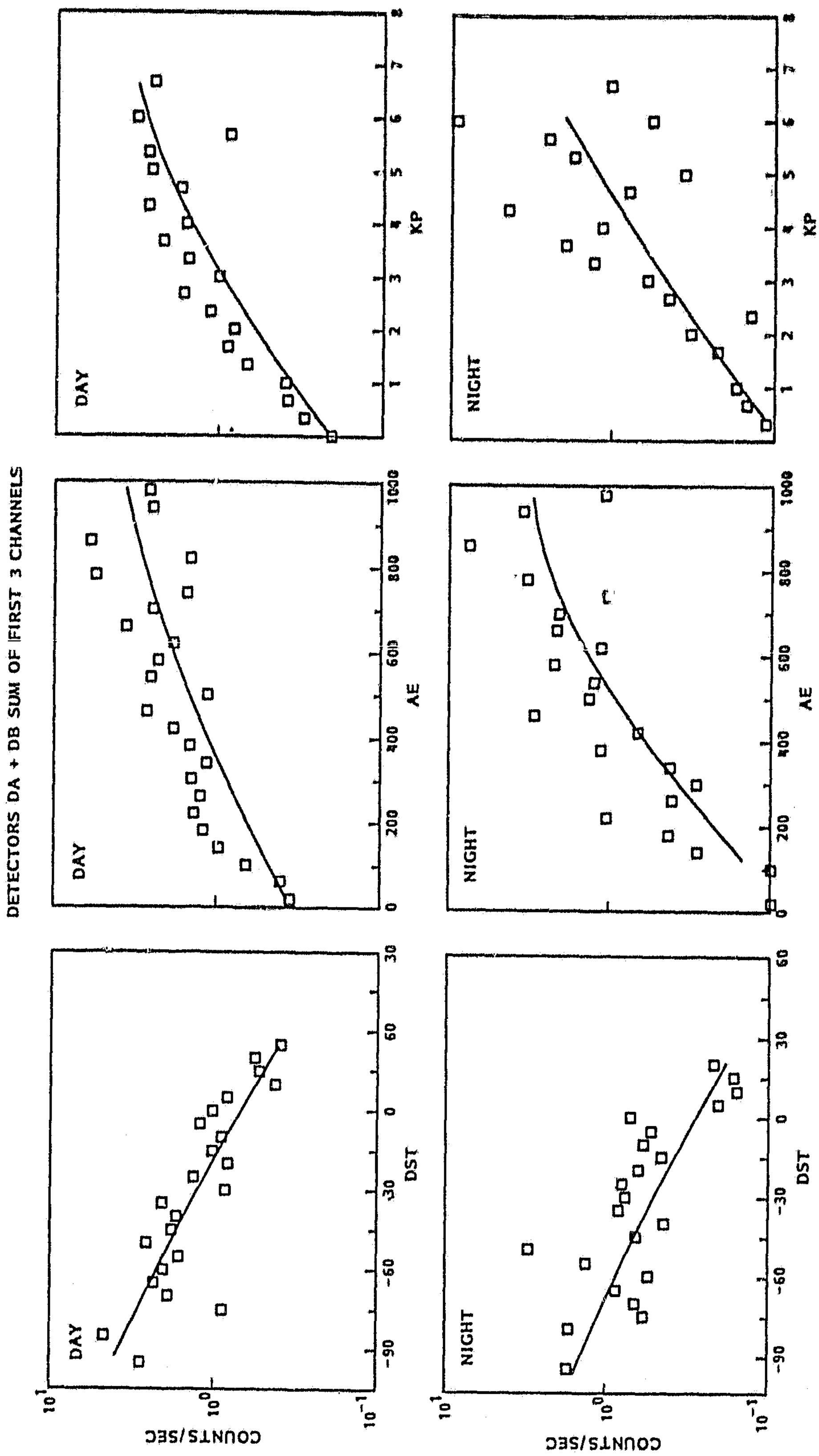

Figure 2A

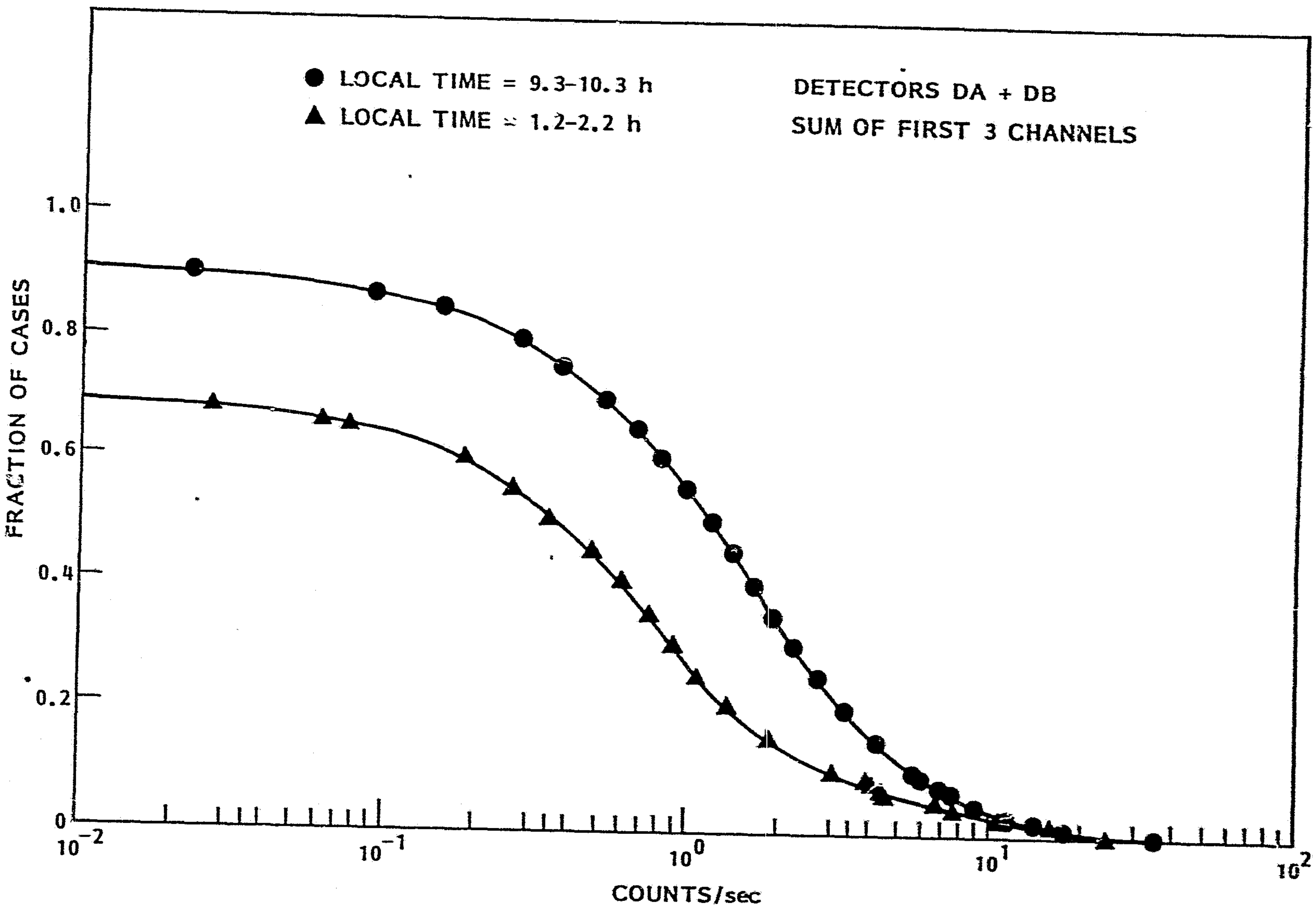
● LOCAL TIME = 9.3-10.3 h
▲ LOCAL TIME ≃ 1.2-2.2 h
DETECTORS DA + DB
SUM OF FIRST 3 CHANNELS
FRACTION OF CASES
1.0
0.8
0.6
0.4
0.2
0
10^-2
10^-1
10^0
10^1
10^2
COUNTS/sec

Figure 2B

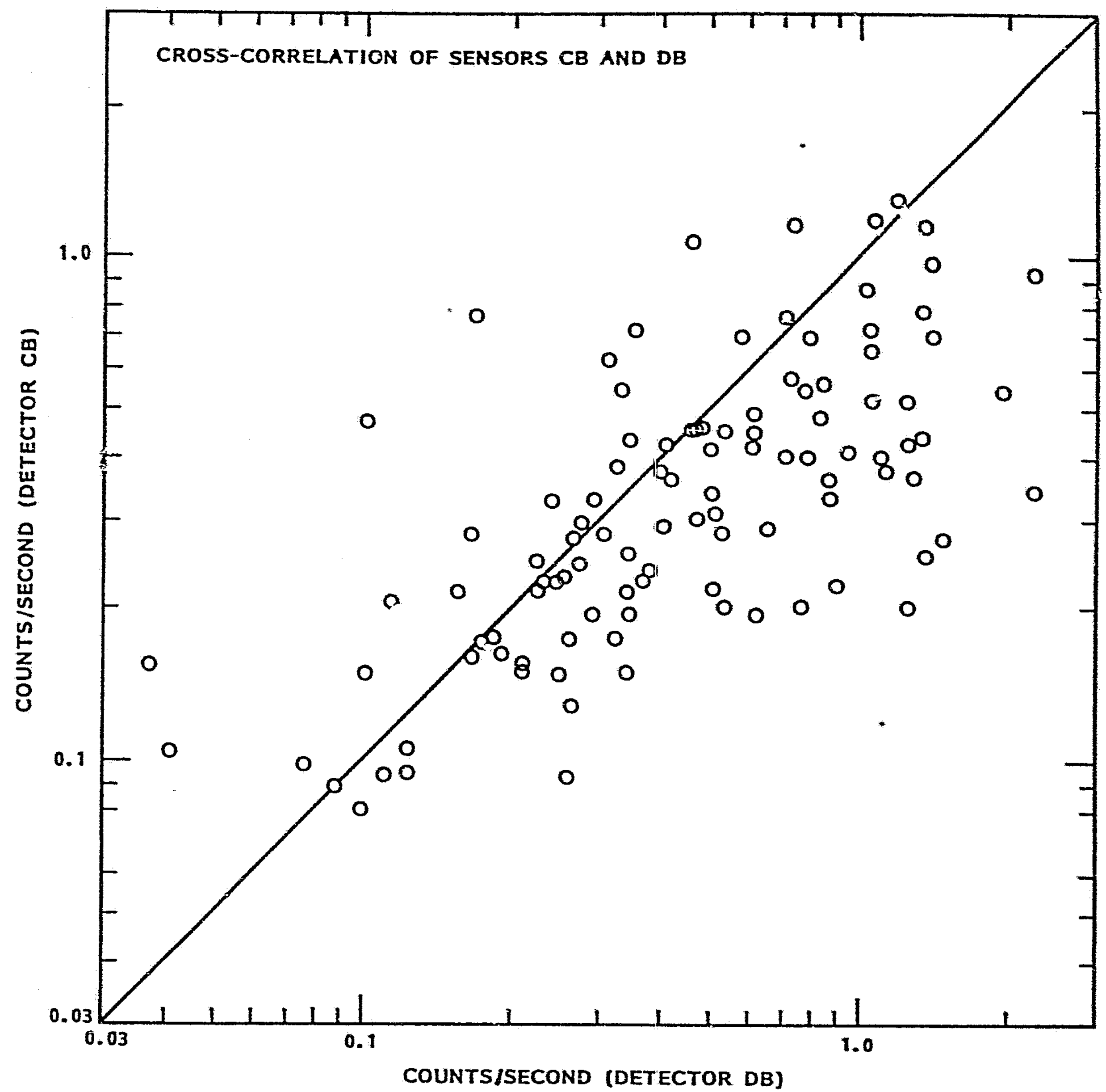

CROSS-CORRELATION OF SENSORS CB AND DB
COUNTS/SECOND (DETECTOR CB)
1.0
0.1
0.03
0.03
0.1
1.0
COUNTS/SECOND (DETECTOR DB)

Figure 3A

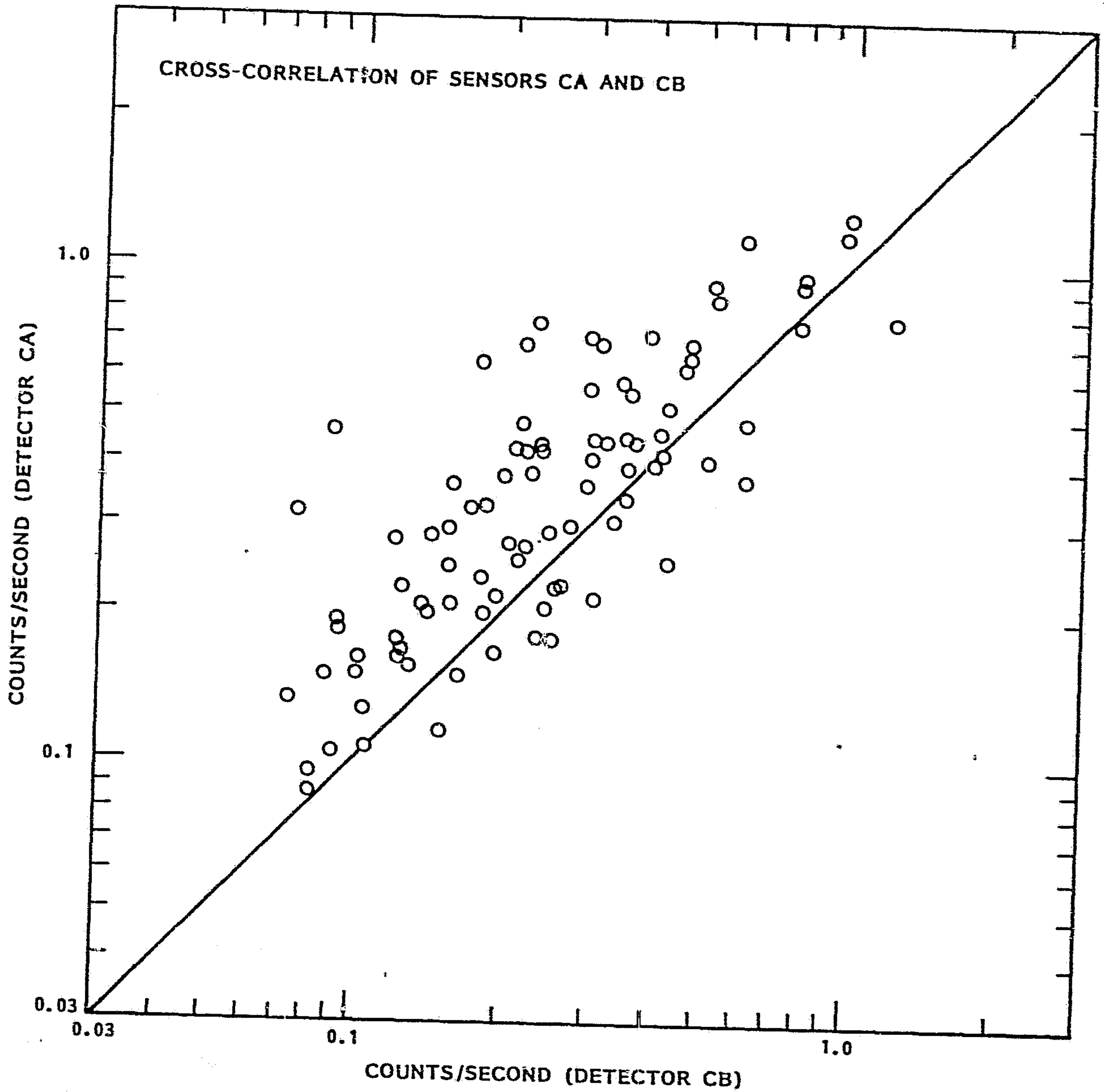
CROSS-CORRELATION OF SENSORS CA AND CB
COUNTS/SECOND (DETECTOR CA)
1.0
0.1
0.03
0.03
0.1
1.0
COUNTS/SECOND (DETECTOR CB)

Figure 3B

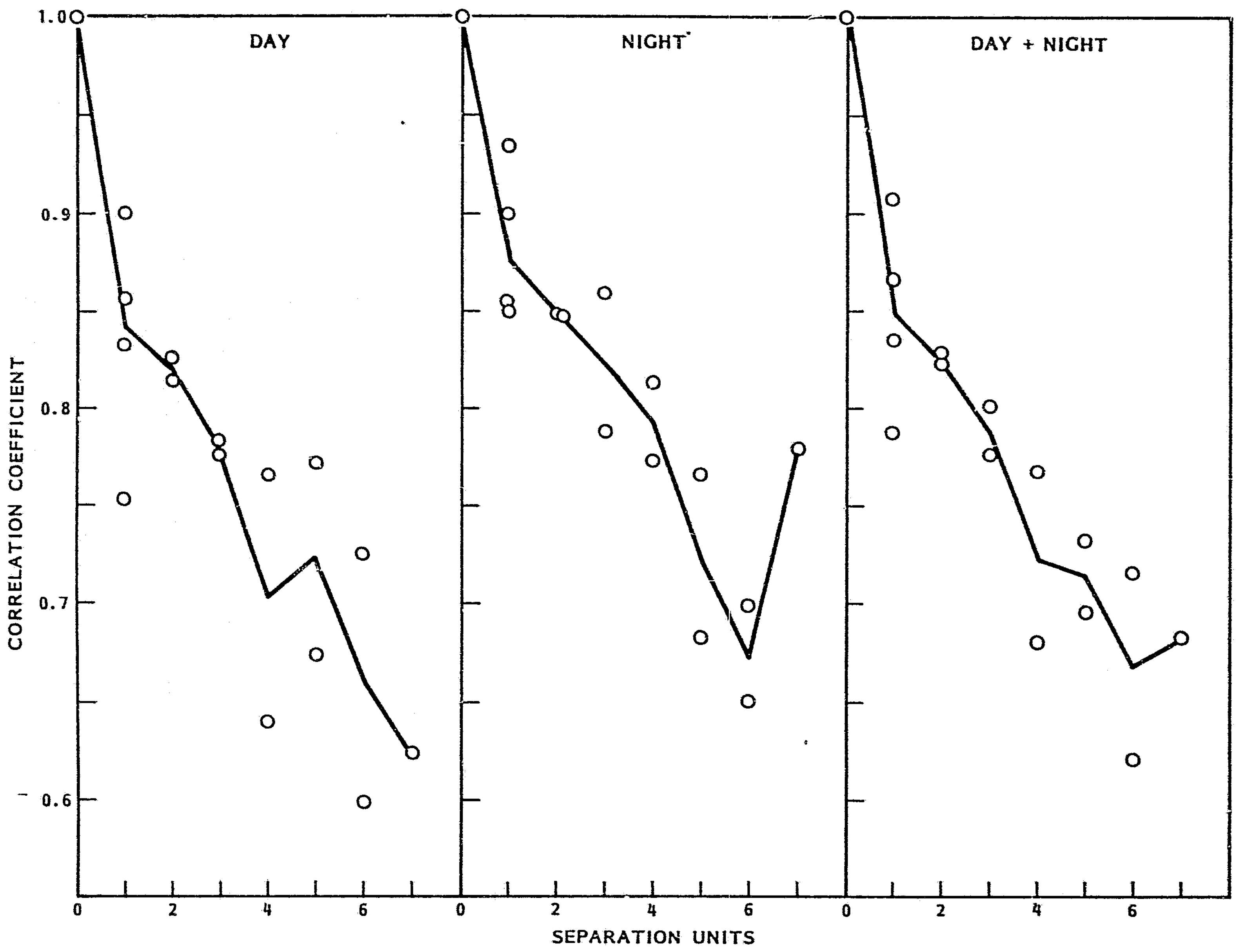
DAY
NIGHT
DAY + NIGHT
1.00
0.9
0.8
0.7
0.6
CORRELATION COEFFICIENT
0
2
4
6
SEPARATION UNITS

Figure 4

ORIGINAL PAGE IS
OF POOR QUALITY

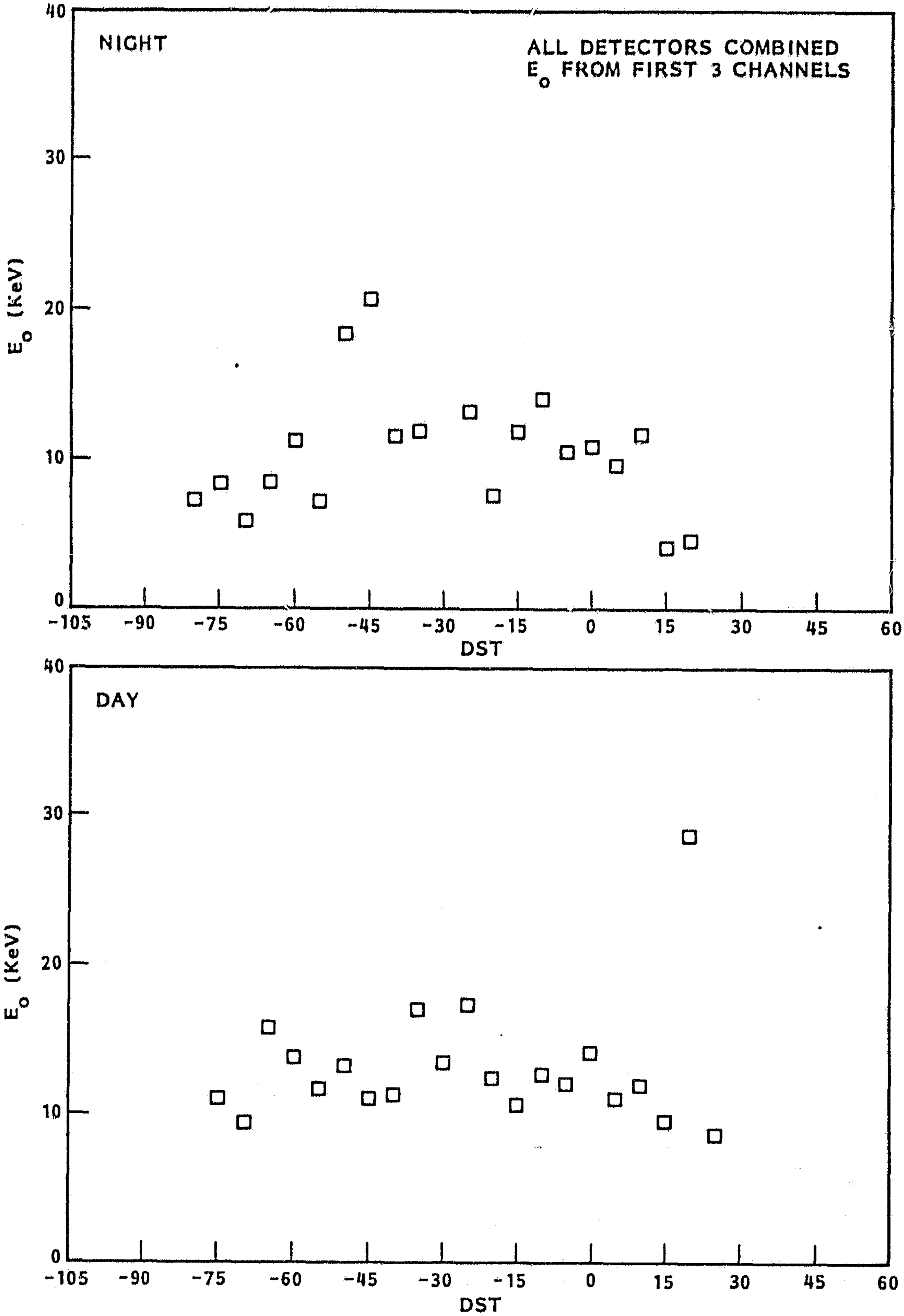

Figure 5

ORIGINAL PAGE IS
OF POOR QUALITY

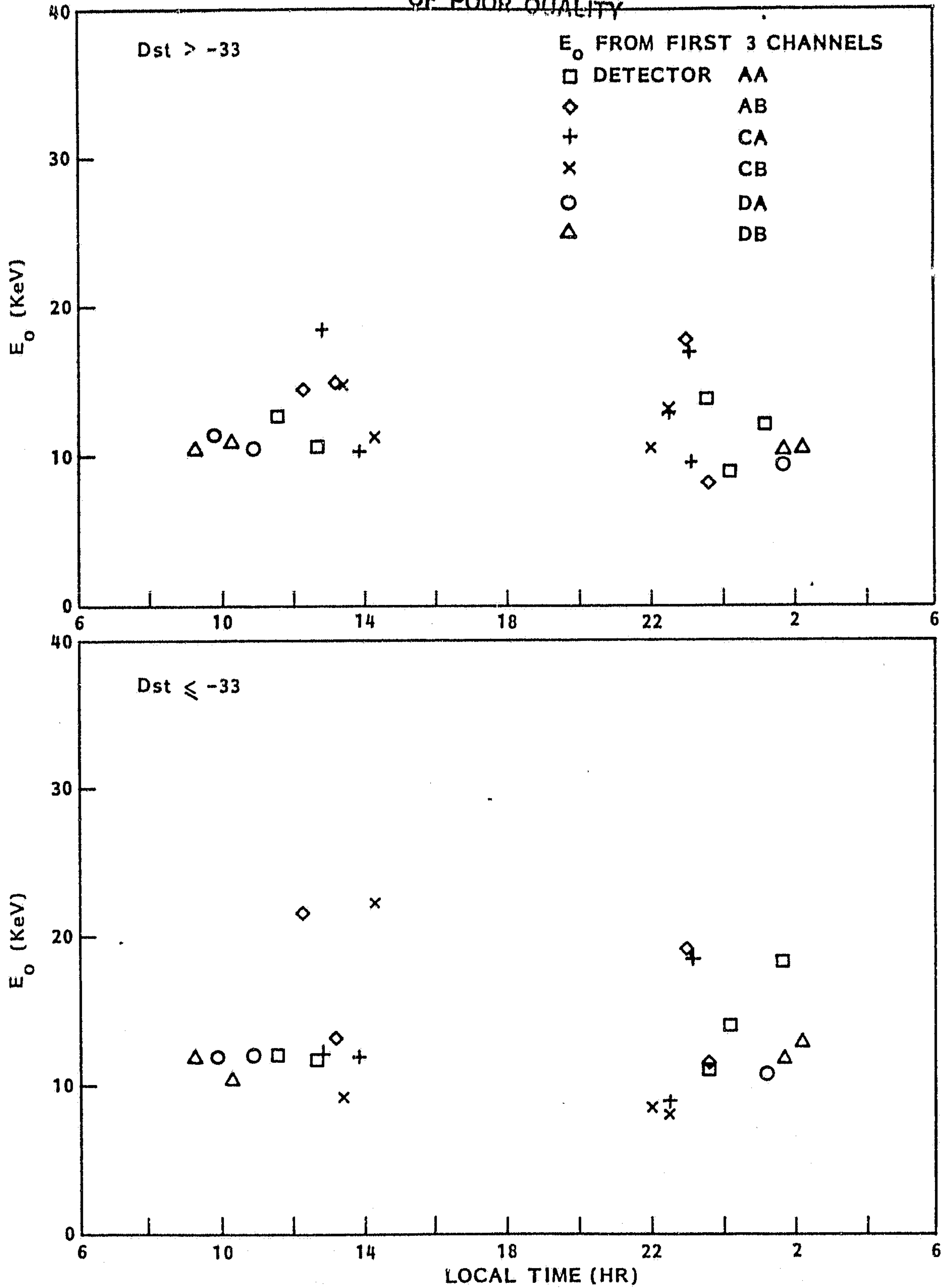

Figure 6

ORIGINAL PAGE IS
OF POOR QUALITY

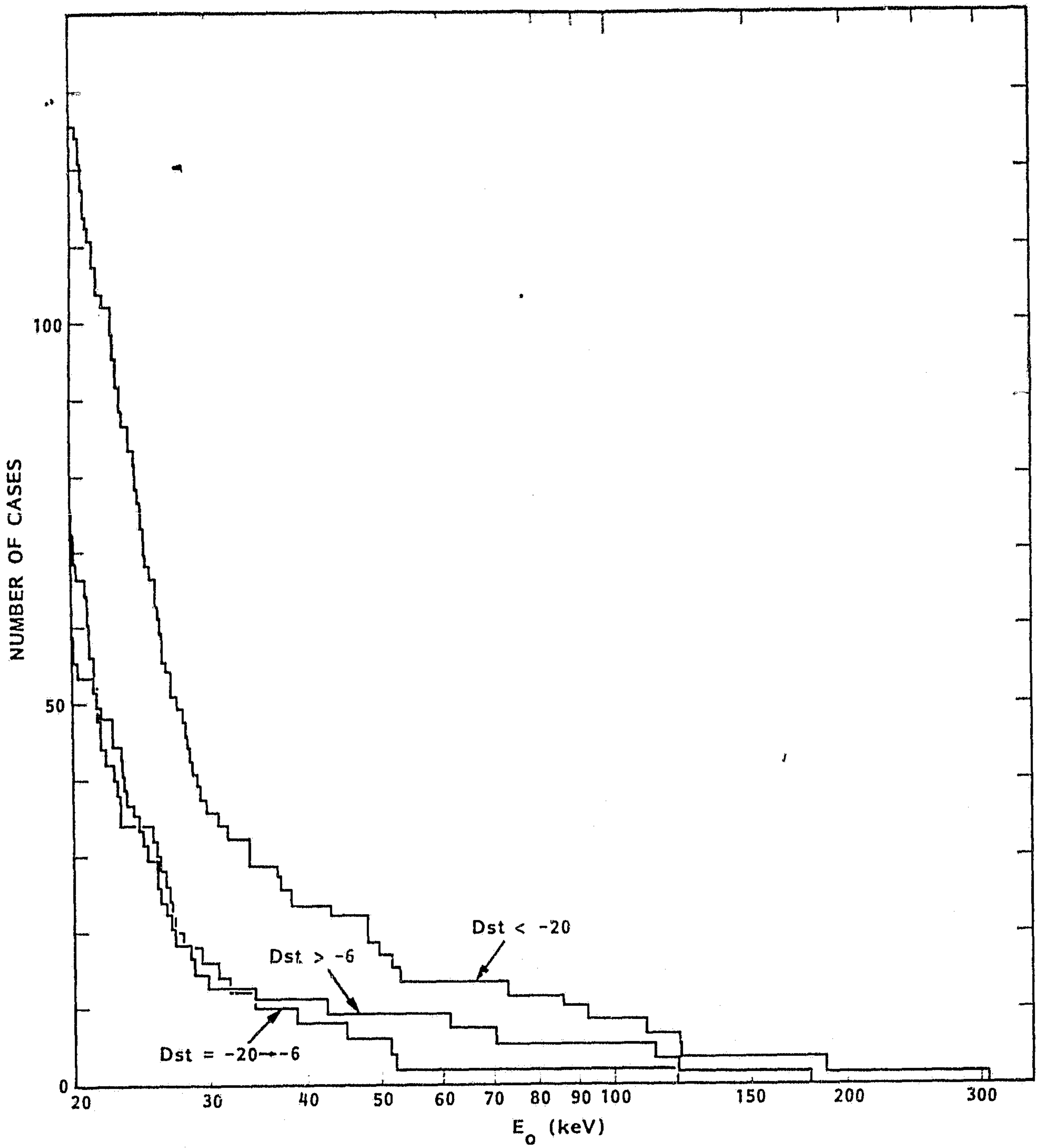

Figure 7

ORIGINAL PAGE IS
OF POOR QUALITY

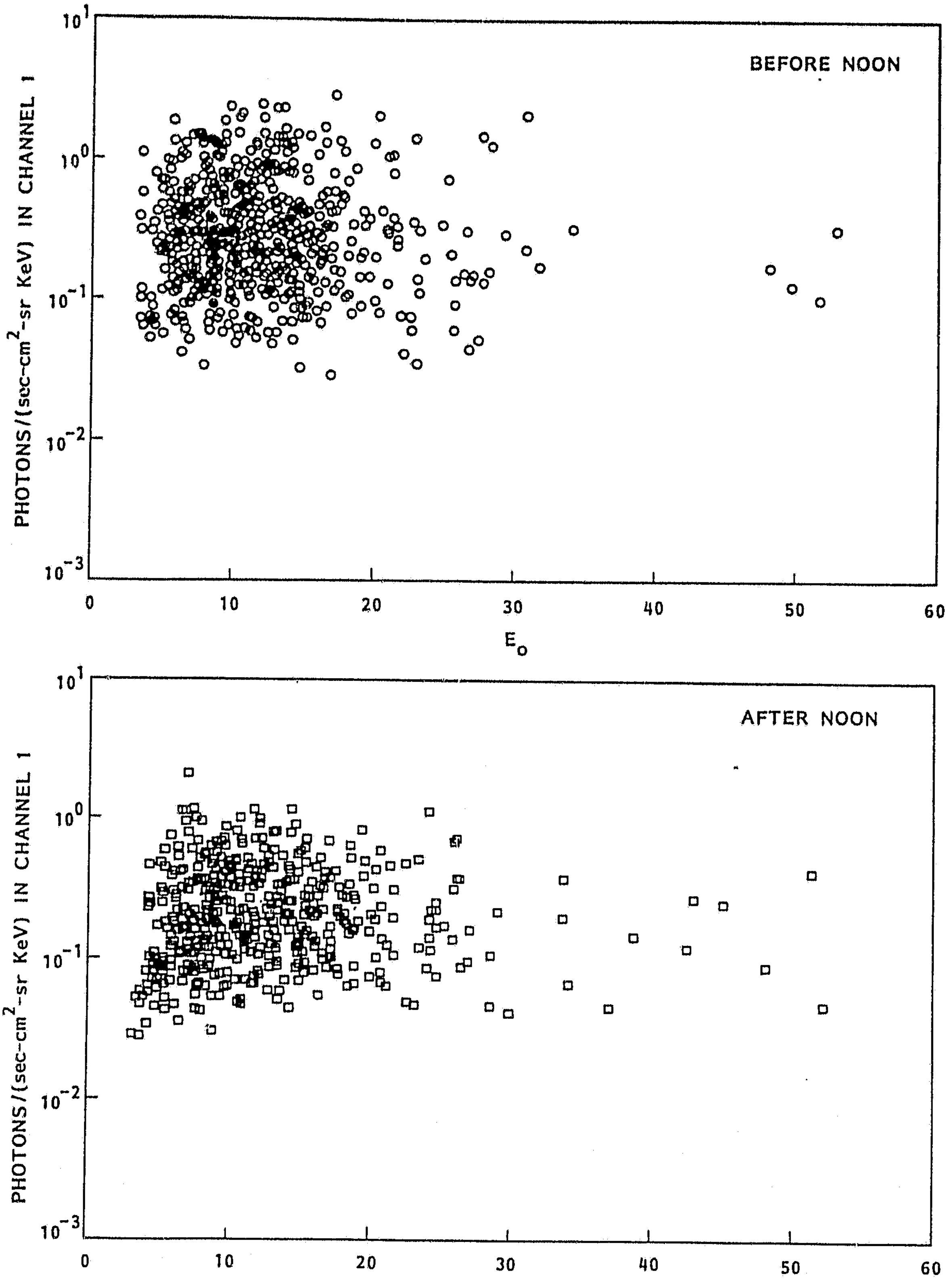

Figure 8A

ORIGINAL PAGE IS
OF POOR QUALITY

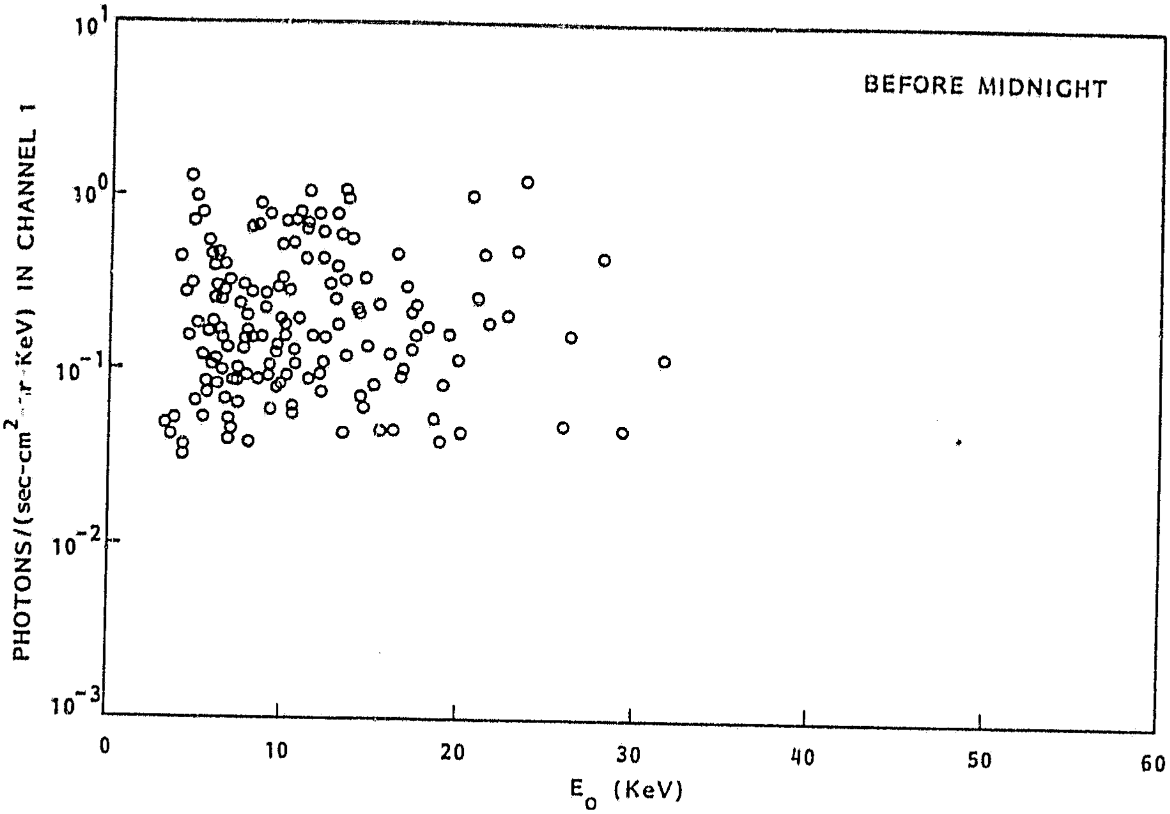

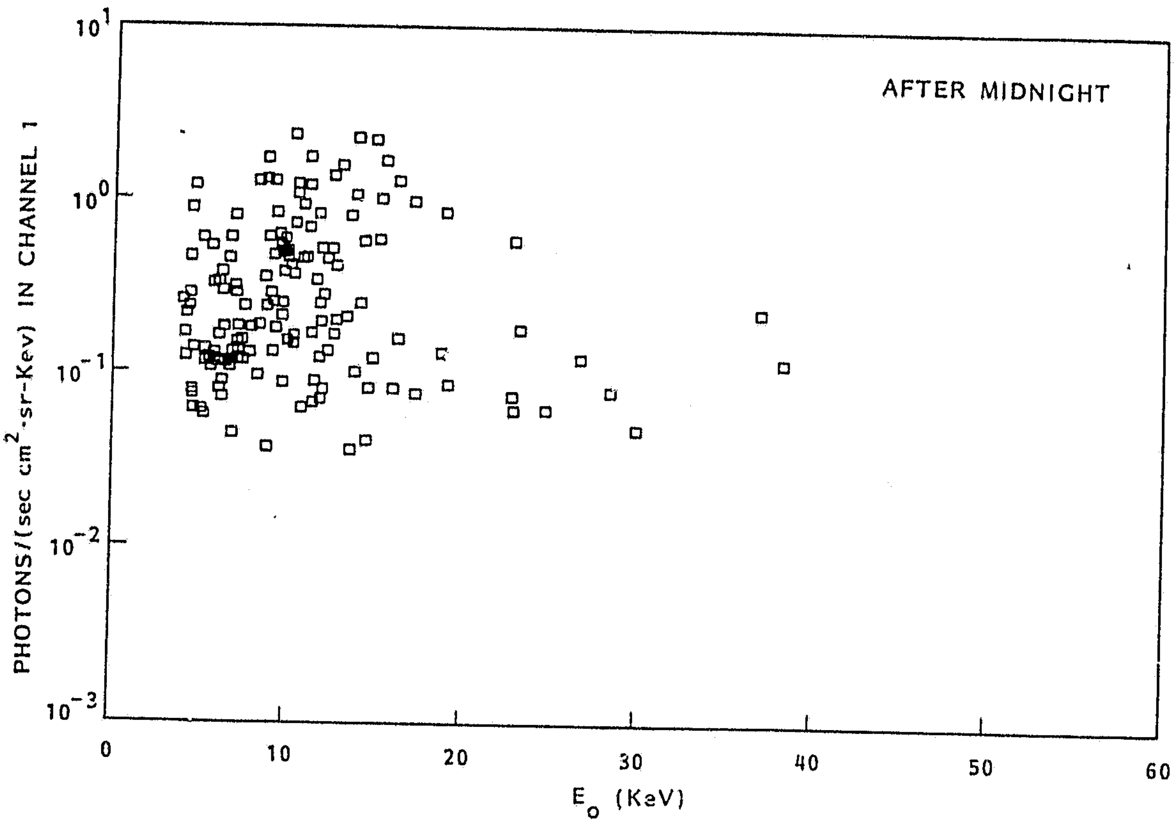

Figure 8B

ORIGINAL PAGE IS
OF POOR QUALITY

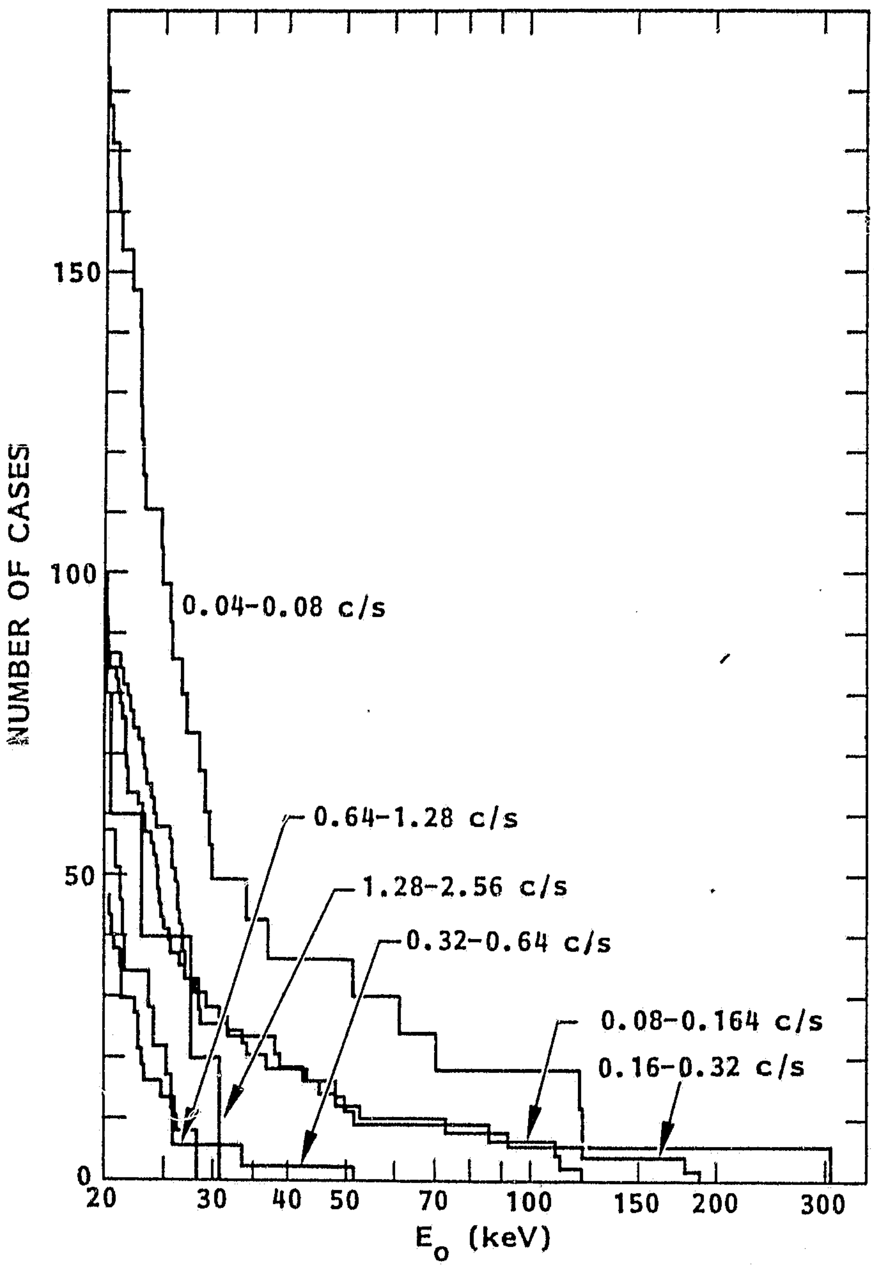

Figure 9

ORIGINAL PAGE IS
OF POOR QUALITY

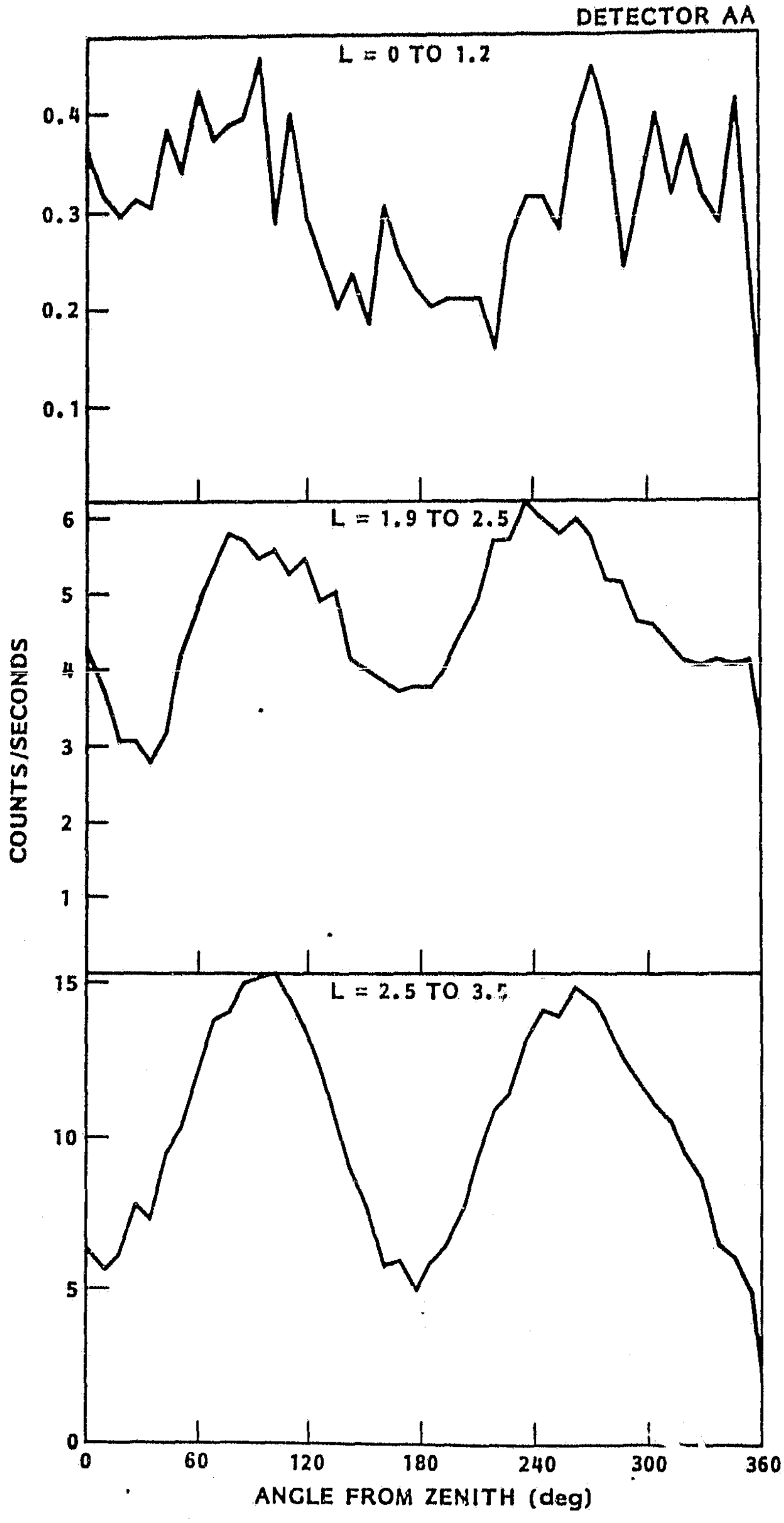

Figure 10


EQUIVALENT BACKGROUND FLUX
GEMS SPECTROMETERS
COUNTS/cm^2-sr-keV-s
10^1
10^0
10^{-1}
10^{-2}
1
1.5
2
3
4
5
6
7
8
9
≥10
L

Figure 11

ORIGINAL PAGE IS
OF POOR QUALITY

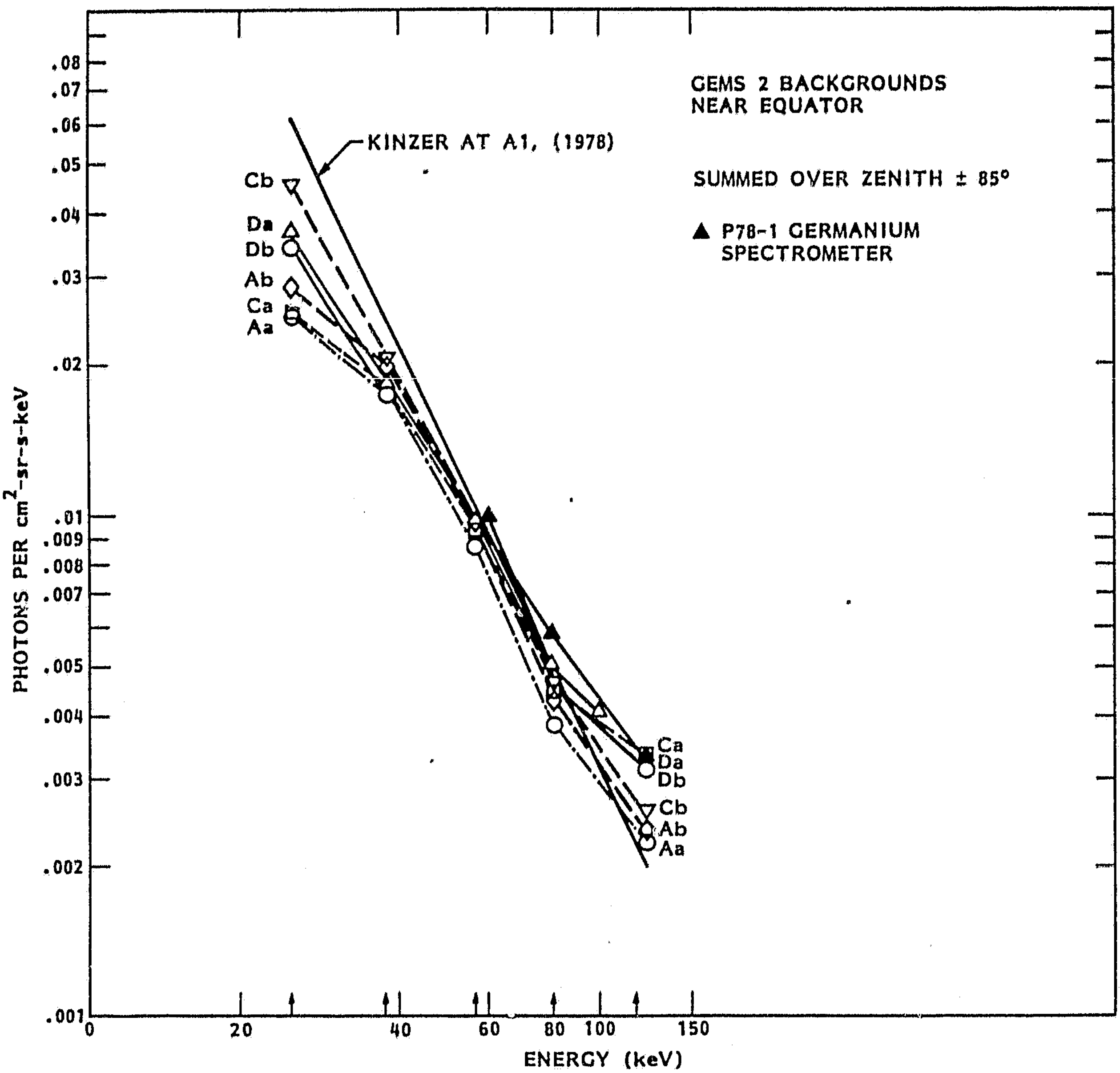

Figure 12